Nature Communications

https://doi.org/10.1038/s41467-026-69427-8

Article in Press

Soft photo-ionotronics

Received: 19 December 2025

Accepted: 2 February 2026

Cite this article as: Liu, X., Adelmund, S.M., Safaee, S. *et al.* Soft photo-ionotronics. *Nat Commun* (2026). https://doi.org/10.1038/s41467-026-69427-8

Xu Liu, Steven M. Adelmund, Shahriar Safaee, Wenyang Pan & Thomas J. Wallin

Soft Photo-Ionotronics

Xu Liu[1], Steven M. Adelmund[2], Shahriar Safaee[2], Wenyang Pan[2], Thomas J. Wallin[1]*

1. Department of Materials Science and Engineering, Massachusetts Institute of Technology, Cambridge, MA 02139, USA

2. Reality Labs at Meta, Redmond, WA 98052, USA

*Corresponding author, email: tjwallin@mit.edu

Abstract

The ability to control the movement of charged species in the circuitry of living beings and machines is essential for complex signal processing, computation, and, ultimately, higher functionality. We describe a class of photo-ion generators (PIGs) based on non-ionic photoacids that can create large (> 1000x) irreversible changes in ionic conductivity under illumination, depending on the PIG species, concentration, and solvent. Incorporation of PIGs into elastomers by simple swelling methods yields soft (60 kPa ≤ E ≤ 10 MPa), stretchable, photo-ionic gels (PIGels). The resolution of photo-patterned conductivity in PIGels is less than 1 cm and demonstrates stability over several days, suggesting utility in engineered devices. Leveraging the photo-responsive properties of these materials, we demonstrate high-sensitivity mechanical sensors via conductance changes ($[\Delta G/G_0]/\sigma = 20$ MPa^{-1}) and photo-writable, soft circuitry.

Introduction

Biology utilizes membranes, ion channels, and intracellular receptors to regulate ionic transport; electronic devices employ diodes, transistors, and amplifiers to direct the flow of electrons and holes. Whereas, biological tissues are often soft and squishy, electronic materials are primarily stiff and inextensible. The field of ionotronics[1-3], or hybrid engineered systems that conduct both ions and electrons, bridges these two regimes. In particular, gel ionotronics[4-6], i.e., where the ionic material is a soft (Young's Modulus, E < 10 MPa) elastomeric gel, enables actuators[7,8], sensors[9,10], and optical displays[11,12] with mechanical properties similar to natural tissues (E_{skin} ~0.6 MPa[13], E_{muscle} ~24.7 kPa[14], E_{brain} ~1 kPa[15]). Such innovative devices can maintain functionality under large deformations (strain, dL/L_0 > 400%[16]) and, consequently, possess broad potential in soft wearable technology, human-machine interfaces, robotics, biomedicine, etc[17-21].

The primary benefit of gel ionotronics is the easy synthesis and manufacture of ionically conductive gels ("ionogels")—such materials are often a polymer network swollen by an electrolyte (e.g., saltwater)[22,23]. Yet, these simplistic gels merely function as simple conductive traces or electrodes; there exists no method to control local ionic conductivity in soft matter ($\boldsymbol{\kappa}$) other than advanced multimaterial manufacturing techniques that encapsulate ionogels in insulative elastomers. To expand the functionality of gel ionotronics and permit dynamic modulation of ionic conductivity within a single soft material, we infuse elastomers with photo-ion generators (PIGs). Upon illumination, solutions of PIGs can produce large and localized changes in ion concentration and consequently ionic conductivity (Λ/Λ_0 > 1000x, f = 1 kHz). Appropriate solvent selection permits integration with elastomers to produce photo-ionic gels (PIGels). As expected, PIGels change from insulative to ionically conductive upon local

stimulation, a key step towards realizing ionic logic in engineered materials at biomechanically relevant regimes (E_{PIGel} > 2 MPa, dL/L_0 > 50%).

Here, we show a general framework for creating soft photo-ionic materials for engineered devices. We describe a class of non-ionic photoacids capable of producing large increases in ionic conductivity (> 1000x) upon illumination. By incorporating such non-ionic photoacids into elastomers via a simple swelling method, we develop photo-ionic gels that combine tissue-like softness (E ~ 2 MPa) with significant, externally triggered signal changes. These materials maintain their functionality under large deformations and exhibit stable, photo-patterned conductivity that persists on the order of days. Highlighting the rich opportunities of this advance, we demonstrate soft, deformable "photo-ionotronic" devices that facilitate the creation of photo-controlled circuits and strain sensors.

Results

Characterization of PIGs in liquid solution

Photoacid generators (PAGs) are chemical species that irreversibly rearrange or cleave upon irradiation to create an acid (A^+, often a proton) and its conjugate base (CB^-)[24,25]. This acid can then catalyze local reactions (e.g., cationic photopolymerization of epoxies), which is particularly useful in photolithography[26], microfabrication[27], and 3D printing[28]. As a result of their utility, there are a myriad of commercially available PAGs that possess different polarities, activation wavelengths, efficiency, etc[29]. Yet, most commercial PAGs are -onium salts (e.g., diaryliodonium or triarylsulfonium cations paired with anions) or zwitterions that are ionically conductive even before illumination. To generate large changes in ionic concentration and thereby conductivity, we identify a class of non-ionic PAGs (i.e., photoacid species initially without charge) that can readily act as photo-ion generators (PIGs). Fig. 1a contains a representative ionic PAG

(triphenylsulfonium triflate, TPST) and three non-ionic PAGs: PIG1: N-hydroxy-5-norbornene-2,3-dicarboximide perfluoro-1-butanesulfonate, (HNDPB); PIG2: N-Hydroxynaphthalimide triflate, (HNT); PIG3: 2-(4-Methoxystyryl)-4,6-bis(trichloromethyl)-1,3,5-triazine, (MBT). Consistent with previous literature[30-33], these species show strong but distinct UV absorption (wavelength of light < 400 nm) and a corresponding change in spectra upon dissociation of the acid, A^+, and conjugate base, CB^- (Fig. 1b).

According to Kohlrausch's law of independent ion migration (equation 1), the total ionic conductivity of a system (Λ_{total}) is the sum of the number of molecules (ν_i) times the molar conductivity (λ_i) for each species in the system. In the simplest system, we only consider the solvent, PAG, photo-generated cation (acid, A^+), and anion (conjugate base, CB^-).

$$\Lambda_{total} = \sum_i \nu_i \lambda_i = \nu_{A^+}\lambda_{A^+} + \nu_{CB^-}\lambda_{CB^-} + \nu_{PAG}\lambda_{PAG} + \nu_{solvent}\lambda_{solvent} \ldots. \quad (1)$$

Where the molar conductivity of a species (λ_i) is equal to the product of the species' mobility (z_i), charge (μ_i), and the Faraday constant (F).

$$\lambda_i = z_i \mu_i F \quad (2)$$

We assume that only a single acid species and conjugate base species form due to the photolysis of the PAG and that the solvent does not change.

$$\nu_{PAG}(t=0) = \nu_{PAG}(t) + \nu_{A^+}(t) \quad where \quad \nu_{A^+}(t) = \nu_{CB^-}(t) \quad (3)$$

Thus, we would expect the change in ionic conductivity to be:

$$\frac{\Lambda_{total}(t)}{\Lambda_{total}\,(t=0)} = \frac{\nu_{A^+}(t)\,\lambda_{A^+} + \nu_{CB^-}(t)\,\lambda_{CB^-} + \nu_{PAG}(t)\lambda_{PAG} + \nu_{solvent}\lambda_{solvent}}{\nu_{PAG}(t=0)\lambda_{PAG} + \nu_{solvent}\lambda_{solvent}}$$

$$= \frac{[\,\nu_{PAG}(t=0) - \nu_{PAG}(t)\,][\lambda_{A^+} + \lambda_{CB^-}] + \nu_{PAG}(t)\lambda_{PAG} + \nu_{solvent}\lambda_{solvent}}{\nu_{PAG}(t=0)\lambda_{PAG} + \nu_{solvent}\lambda_{solvent}} \quad (4)$$

Fig. 1c correlates this photoacidity to ionic conductivity as a function of photo-exposure at an AC driving frequency, f = 1 kHz. At the same concentration (0.1 M) and solvent (DMSO), the non-

ionic PAGs exhibit orders of magnitude relative changes in ionic conductivity ($\Lambda(t)/\Lambda_{0,MBT} > 1800$, $\Lambda(t)/\Lambda_{0,HNT} > 400$, $\Lambda(t)/\Lambda_{0,HNDPB} > 10$) upon illumination. By comparison, the ionic PAG shows negligible change ($\Lambda(t)/\Lambda_{0,TPST} > 1.1$), as expected due to ionic dissociation of the onium salt without illumination ($\Lambda_{0,TPST}$ ~2000 μS cm^{-1}, see Supplementary Fig. 1 and 2 for full data). The data support our hypothesis; the largest changes in conductivity result by selecting photoacids and solvents with the smallest initial molar conductivities. We call the PAG species that produce such large changes in ionic conductivity PIGs. While not all inclusive, we propose that most non-ionic PAGs readily function as PIGs.

Our observed photo-ion effect is multifaceted and depends on the complex interactions between the PIG, solvent, AC driving frequency, and the spectrum of light (see Supplementary Information Section 1 for a more thorough explanation of these considerations). While the details of a material system will determine which PIG is ideal for a given application, we focus this study on PIG3 (MBT) due to its attractive combination of high solubility in common solvents (Supplementary Table 1), sensitivity to longer, less damaging UV-A wavelengths (λ = 365 nm, see Fig. 1b), and low relative cost (~$15/g). Similarly, despite the high solubility of MBT (0.21 M) and greater change in ionic conductivity in volatile solvents like acetone ($\Lambda/\Lambda_{0,MBT} > 4000$, f = 1 kHz, see Supplementary Fig. 3), the high vapor pressure of such PIG solutions makes practical implementation difficult. For that reason, we select DMSO as our working solvent for the remainder of the study.

As shown in Fig. 1d, increasing the concentration of PIG3 over three orders of magnitude does not produce proportional increases in the change in ionic conductivity under illumination (see Supplementary Fig. 4 for full data). As we observe similar initial dark (i.e., $H_e = 0$) conductivities across concentrations, the lack of proportionality suggests incomplete photo-dissociation at higher

concentrations. In Fig. 1f, the observed molar conductivity (Λ_m) is not linear with the square of the concentration ($\sqrt{c}$) regardless of light dosage, which is a characteristic of weak electrolytes. For comparison, we include generalized strong electrolyte behavior according to the Debye-Hückel-Onsager theory (Equation 5) where Λ_m^0 is limiting molar conductivity at infinite dilution, A is an empirical constant, and c is electrolyte concentration[34].

$$\Lambda_m = \Lambda_m^0 - A\sqrt{c} \qquad (5)$$

While weak electrolyte behavior limits the maximum PIG conductivity change to ~1000x, it also explains why a similar photo-ion effect exists at low concentrations and photo-exposures. Such behavior is desirable for applications requiring rapid changes in conductivity with minimal changes in the system composition.

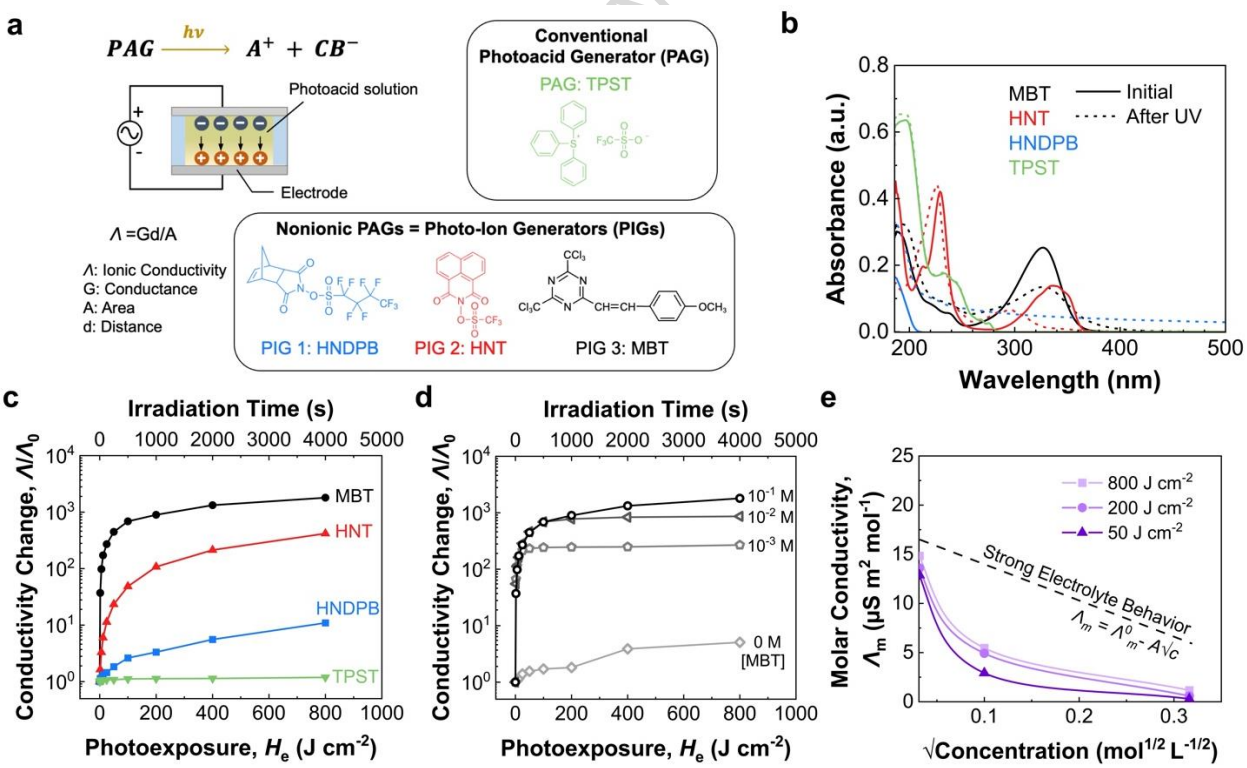

Fig. 1 | Ionic conductivity measurement and photoacid in DMSO

a, Overview photoacid generators (PAG) and non-ionic photoacid generators (photo-ion generators, PIGs) with the schematic for measuring ionic conductivity. **b,** UV-Vis spectra of MBT, HNT, HNDPB, and TPST (0.0001 M in

acetonitrile) before and after UV exposure. **c,** Average (n = 9) ionic conductivity change at f = 1 kHz of 0.1 M MBT, HNT (light source = 365 nm LED), HNDPB, and TPST (light source = Hg lamp) DMSO solution as a function of photo-exposure. **d,** Average (n = 9) ionic conductivity change at f = 1 kHz of 0, 0.1 M, 0.01 M, and 0.001 M MBT in DMSO under photo-exposure (light source = 365 LED). **e,** Average (n = 9) molar conductivity of MBT in DMSO at varying photo-dosages and concentrations showing weak electrolyte behavior, and general behavior of a strong electrolyte.

Fabrication and properties of PIGels

We immerse polyurethane rubber (PUR) in a PIG solution to create photo-ionic gels (PIGels). A favorable interaction between the DMSO and PUR allows the PIG solution to swell the polymer network until it reaches equilibrium (Fig. 2a), i.e., when the elastic potential energy of the swollen gel offsets the chemical potential of the solution in the gel. Our choice of the swelling method to fabricate the PIGels provided a simple and scalable approach for incorporating MBT into the polymer system. This method is applicable to a wide variety of polymer systems. Fig. 2b shows the kinetics of swelling for disks (d_0 = 19 mm, h_0 = 0.5 mm) of PUR soaked in 0.1 M solution of PIG3 in DMSO. At 1000 min, the swelling ratio (SR) is approximately 90% which corresponds to a PIG concentration of ~2.6 wt% in the PIGel, assuming uniform composition. At 2.62 wt% loading, the PIGel exhibits a significant conductivity change of $>$ 300x after 40 J cm^{-2} irradiation (Fig. 2c, see Supplementary Fig. 5 for data for all concentrations and exposure dosages). However, this effect is much smaller in the PIGel than in the solution ($\Lambda/\Lambda_0 >$ 1000x). As the initial conductivity prior to photo-exposure is similar in both the PIGel and the PIG solution (see Supplementary Fig. 4, 5), we posit that the reduction arises predominantly from a drop in ionic mobilities (Equation 2) and not the contribution of mobile ions from the PUR. Such findings are unsurprising, given that ion mobility generally decreases in more viscous environments[35].

Additionally, loading the PUR with PIG solution alters the polymer network configuration and changes the macroscopic mechanical properties. Typically, as a gel swells, the volumetric crosslink density decreases, which produces a corresponding decrease in the Young's modulus, *E*. As the PIG loading increases from 0 to 2%, the PIGel's modulus decreases from 3.3 to 2 MPa, approximately that of human skin[36] (Fig. 2d). Unfortunately, as shown in Fig. 2e, the ultimate strain decreases from 175% to 25% at a swelling ratio of 90%. This drop in performance is not surprising, as Lake-Thomas theory[37] suggests fracture energy is proportional to the areal chain density in a plane. We also consider the effect of illumination on mechanical properties. In Fig. 2d and e, we measure a slight softening and embrittlement of the gel after irradiation. We hypothesize this behavior stems from a decrease in the effective crosslink density that occurs due to the combined effects of polyurethane photolysis (e.g., chain scission) and the newly generated ions disrupting hydrogen bonding in the urethane linkages. To maintain an ultimate elongation > 100%, we target lower swelling ratios (e.g., SR ~12%, PIG concentration ~0.48%) for practical use as the material is still robust to manipulation (Fig. 2f). Again, due to the weak electrolyte behavior, low loadings still produce significant ionic conductivity changes of approximately two orders of magnitude (Fig. 1d).

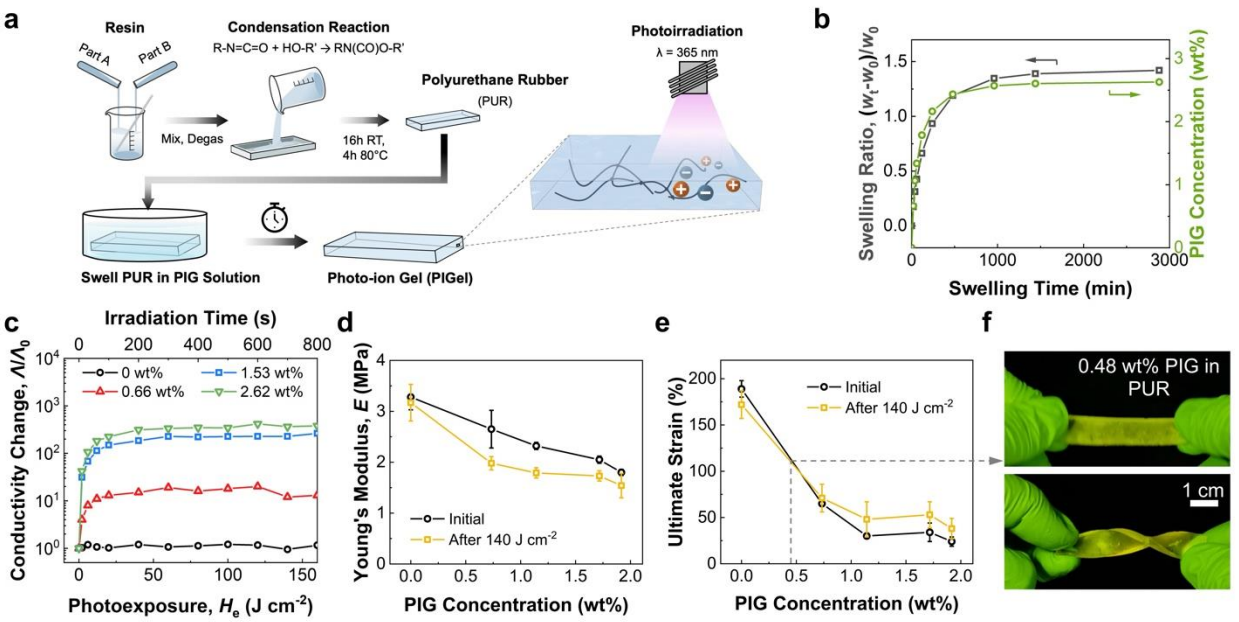

Fig. 2 | Preparation and properties of PIGels based on Clear Flex 50 with MBT

a, Process for fabricating PIGels. **b,** Average (n=7) swelling behavior of Clear Flex 50 disks (d_0 = 19 mm, h_0 = 0.5 mm) with 0.1M MBT in DMSO solution. **c,** Average (n = 9) conductivity change (f = 1 kHz) of these PIGel with 0, 0.66 wt%, 1.53 wt%, 2.62 wt% PIG concentration as a function of photo-exposure (light source = 365 nm LED). **d,** Young's Modulus of MBT based PIGels before and after 140 J cm^{-2} photo-exposure (light source = 365 nm LED). Data are presented as mean values with error bars representing standard deviation, n = 7. **e,** Ultimate Strain change of MBT based PIGel before and after 140 J cm^{-2} photo-exposure (light source = 365 nm LED). Data are presented as mean values with error bars representing standard deviation, n = 7. **f,** Representative image of compliant PIGel under 12% swelling ratio.

Importantly, our PIGel framework is largely independent of the underlying polymer network chemistry which allows for additional tunability of material properties through selection of the host polymer. To demonstrate this capability, we fabricated gels using a family of polyurethane elastomers with varied mechanical properties: Clear Flex 30 (soft, Shore A ~ 30), Clear Flex 50 (intermediate, Shore A ~ 50), Clear Flex 95 (stiff, Shore A ~ 95), as well as VHB (very high bond) viscoelastic acrylic foam (see Supplementary Fig. 6 and 7). As shown in Figure 3, the choice of elastomer directly impacts the PIGel's performance across numerous interrelated

metrics, e.g. stiffness, swellability, and ionic conductivity change (see Supplementary Information for a discussion). As expected, the softer, more loosely crosslinked materials exhibit higher swelling ratios in the PIG solution (Figure 3a). (Figure 3b). However, in the case of Clear Flex 30, its high initial conductivity prior to photoirradiation leads to a smaller signal change (see Supplementary Fig. 8). As shown in Figure 3c, PIGels combine tissue-like softness (E<10 MPa) with a significant, externally triggered signal change, overcoming the common trade-off between mechanical compliance and functional conductivity. This makes the PIGel platform a promising material for soft devices, such as wearables, that mimic the functionalities of biological tissues.

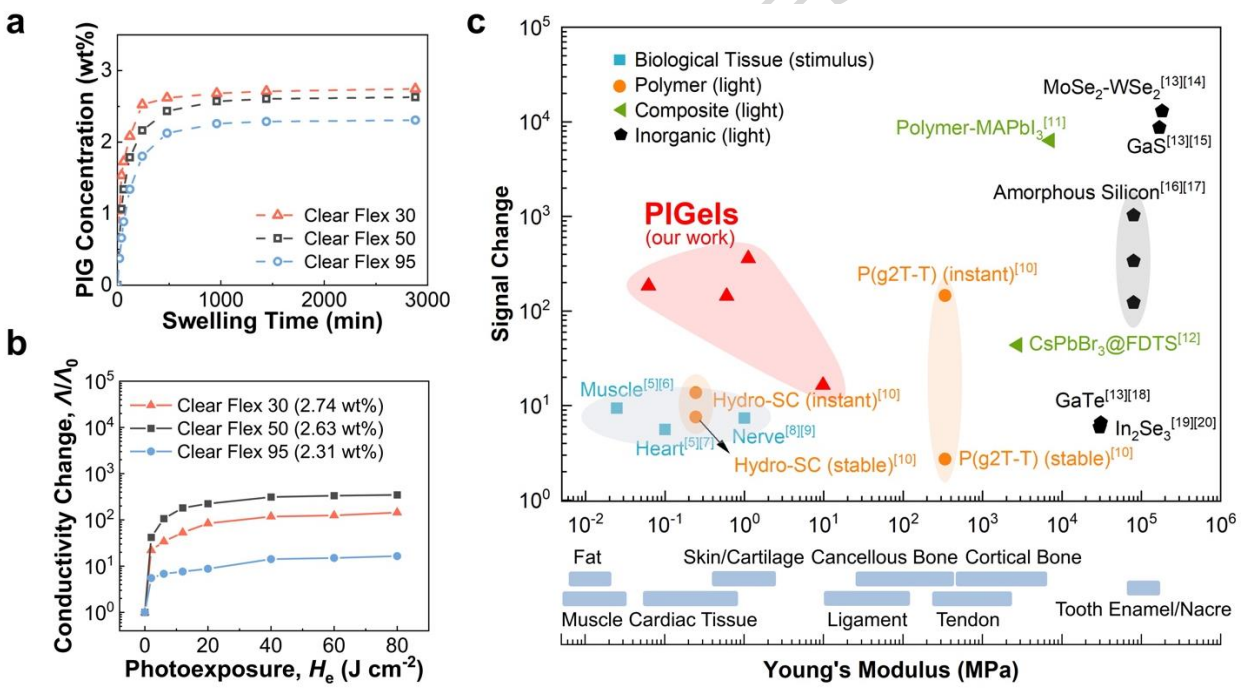

Fig. 3 | Conductivity improvement of different MBT polymer systems

a, Average (n=5) swelling behaviour of Clear Flex 30, 50, and 95 disks (d_0 = 19 mm, h_0 = 0.5 mm) with 0.1M MBT in DMSO solution. **b,** Average (n = 9) conductivity change (f = 1 kHz) of these saturated PIGels after 2800 mins swelling as a function of photo-exposure (light source = 365 nm LED). **c** Comparison of dynamic response and the elastic nature of biological tissue, polymer, composite, and inorganic (left dot is VHB-based PIGel, bottom dot is Clear Flex 95-based PIGel, top dot is Clear Flex 50-based PIGel, central dot represents Clear Flex 30-based PIGel.

Resolution and stability of photo-patterned PIGels

For suitable performance in a device, the PIGel must exhibit photo-patterned conductivity that maintains its resolution on relevant lengths and timescales. In Fig. 4a, we illuminated (H_e = 200 J cm^{-2}, λ = 365 nm) a 3 mm strip of the PIGel and measured the resistance between evenly spaced pins both perpendicular to and along the path of exposure. As expected, the illuminated path exhibits a resistance two orders of magnitude less than that measured 1-2 and 2-3 cm away (Fig. 4b). For distances 0-1 cm away from the path of conduction, we measure a smaller 30x change in resistance; we attribute this slight increase in conductance to the photo-patterned line's non-zero thickness (t = 5 mm) which results in some photo-generated ions between these two pins. Still, for all positions, we observe that the ionic conductivity is stable on the length scale of days and the photo-generated ions have a relatively low diffusivity of 3.79×10^{-6} cm^2/s in our polyurethane rubber (see Supplementary Information Section 3 for calculation), which suggests diffusion of ions beyond the photo-pattern is slow enough to enable practical utility in devices. Although this diffusion would result in a time-dependent loss of photopatterned resolution, as expected, it is ~30x slower than that of protons in bulk aqueous solution due to interactions between the ions and the polyurethane chains, which likely restrict their free diffusion. We similarly observe excellent shelf stability for the unexposed PIG solutions (see Supplementary Fig. 10).

Applications in soft sensors and photopatterned circuitry

The photo-responsive behavior of PIGels enables the construction of soft photo-ionotronic devices for numerous applications. In conventional soft robots, ionogels often act as simple strain sensors[22]. Fig. 4c highlights the ability of PIGels to function in a similar capacity. Compared to the initial gel, photo-patterning a PIGel produces a large change in conductance (ΔG) with

deformation. This corresponds to an over 60x enhancement in strain sensitivity for the small strain regimes (dL/L_0 = 5%) before and after illumination. When considering the softness of the PIGel, this change in conductance represents an effective sensitivity ($[\Delta G/G_0]/\sigma$) of 20 MPa^{-1}, implying utility for high resolution sensing even in low stress regimes. Another immediate application of PIGels is for selective patterning of circuitry in soft matter. To demonstrate this capability, we inserted three LEDs at different locations into a PIGel. As shown in Fig. 4d, 4e, and Supplementary Video 1, brief illumination allows us to trace a path of conduction from the source electrode to each LED. As a result, we can control the soft circuit and activate each LED at a desired location and time.

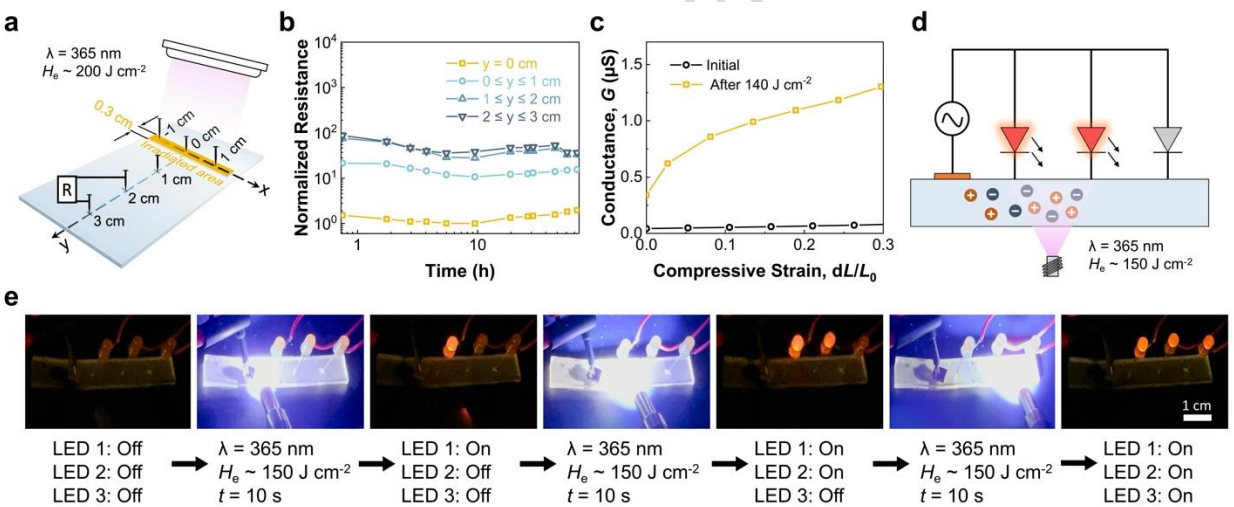

Fig. 4 | Demonstration of PIGels

a, Experimental setup for measuring conductive resolution of photo-patterned PIGel. b, Normalized resistance change (*f* = 1 kHz) as a function of time post-irradiation of photo-patterned PIGel. c, Average (n = 3) conductance change (*f* = 1 kHz) of PIGel under deformation. d, Schematic of dynamic photo-patterning of

a soft, stretchable circuit. e, Time series of photo-patterning of conductivity in a PIGel leading to the progressive illumination of LEDs ($V_{applied}$ = ±100 V, f = 1 kHz).

Discussion

We have shown a general framework for creating soft photo-ionic material in engineered devices. Solutions of non-ionic photoacids act as photo-ion generators to create large ($\Lambda(t)/\Lambda_0$ > 1000x) changes in ionic conductivity in response to illumination. These PIGs function as weak electrolytes, which allow for significant changes in conductivity under illumination in even dilute solutions. As a result, these PIGs can be swollen into elastomers like polyurethane rubber to create PIGels that maintain their conductivity ($\Lambda(t)/\Lambda_0$ > 100x) in soft (E ~ 2 MPa), stretchable (dL/L_0 > 100%) form factors. The photo-patterned ionic conductivity is stable across cm length scales on the order of days. Thus, PIGels can be utilized to make myriad devices, including strain sensors with high sensitivity ($[\Delta G/G_0]/\sigma$ > 20 MPa^{-1}) and photo-patternable soft circuits.

In all likelihood, more ideal combinations of polymer, solvent, and PIGs exist than those surveyed in this initial work (see Supplementary Table 1). Future compositions should seek to improve photo-dissociation and solubility to maximize change in conductivity while minimizing deleterious mechanical effects of highly swollen gels. In fact, it may be possible to remove the solvent altogether and tether the photo-ionic moieties as side groups into the polymer backbone of the elastomer, though this may correspond to a precipitous drop in ionic mobilities. The photo-ionic effect exploited here likely exists in other classes of materials beyond non-ionic photoacids; for example, photo-degradable chelating agents could release attached metal ions to similar effect[38,39]. Additionally, this work only demonstrates a one-way ability to "turn on" ionic conductivity. A class of metastable photoacids (mPAH) exists where the acid and conjugate base recombine on the time scale of seconds or in response to photo-stimulation[40]. Thus, an appropriate

non-ionic mPAH species could give rise to reversible photo-ionic behavior that ultimately leads to soft photo-ionic transistors and dynamic control of ionic circuits.

Methods

PIG solution preparation

We prepared all samples in amber light conditions to avoid the potential influence of ambient UV light exposure. All solutions were stored in amber bottles, and we added molecular sieves to dry the solvents prior to use. To test the ionic conductivity of different photoacids, we prepared 10 mL, 0.1 M photoacid solution with different photoacids, including 2-(4-Methoxystyryl)-4,6-bis(trichloromethyl)-1,3,5-triazine, N-Hydroxyphthalimide triflate, N-Hydroxy-5-Norbornene-2,3-dicarboximide perfluoro-1-butanesulfonate, and Triphenylsulfonium Triflate. Solutions were stirred with a vortex mixer (10,000 RPM) to fully dissolve the powder. To obtain the ionic conductivity as a function of concentration 2-(4-Methoxystyryl)-4,6-bis(trichloromethyl)-1,3,5-triazine in DMSO solution, we prepared 10 mL photoacid solution at 0.1 M, 0.01 M, and 0.001 M.

PIGel preparation

We made sheets of polyurethane rubber (PUR) from Reynold's Advanced Material's Clear Flex 50 per manufacturing guidelines. Briefly, we dispensed part A and part B at a 1:2 mass ratio into a mixing cup prior to stirring by hand for one minute. We then mixed at 2000 rpm under vacuum in a planetary mixer (FlackTek DAC 1200-500V) for 3 minutes, poured into a new container, and stirred again by hand for one minute. We repeated planetary mixing under the same protocol, poured the resin into a Teflon-coated aluminum mold, and cured it in a pressure pot (dP = 60 psi) for 16 h. To ensure full conversion of the condensation reaction, we transferred the mold to an 80 ℃ oven for at least 2 h before demolding. To obtain PIGels, we soaked the resulting

rubber in a 0.1 M PIG3 solution for targeted periods of time. After removing the PIGel from the solution, we minimized solvent evaporation by storing it in a closed container with a saturated DMSO atmosphere.

Ionic conductivity measurements

We measured the conductance with a Discovery HR-2 hybrid rheometer equipped with a dielectric spectroscopy accessory. For the PIG solutions, we use a custom glass gasket (*ID* = 15 mm, *OD* = 25 mm, *h* = 1.7 mm) placed on the bottom electrode of the rheometer to prevent fluid loss and reduce evaporation (see Supplementary Fig. 11). We then pipette in 0.7 mL of solution, bring the top electrode into contact with the gasket. We then conduct a frequency sweep (10 Hz < *f* < 1 MHz) at 2 V with an electrode gap of 1700 μm to measure the conductance. For PIGels, we placed the material directly on the electrodes without a gasket. The electrical properties of the PIGel samples were characterized via an Anton Paar MCR series rheometer (Model 302, H-PTD200) equipped with a Dielectro-Rheological Device (DRD) attachment. All measurements were performed at a controlled temperature of 25.0±0.1 °C using a 50 mm diameter titanium parallel-plate (PP50/DI/TI) measuring system. PIGel samples were punched as disks with an initial diameter of 19.0 mm and a thickness of 0.50 mm. To ensure consistent and reliable electrical contact across the sample-electrode interface and to account for variations in sample thickness post-swelling, a constant axial compression force of 1.0 N was applied and maintained throughout the measurement. Gel dimensions were measured with calipers immediately prior to the experiment. We repeated each test nine times and reported the average value (see Supplementary Fig. 8 and 9 for full data).

We calculate ionic conductivity from conductance using the following relationship:

$$\Lambda = \frac{\mathrm{Gd}}{\mathrm{A}} \qquad (6)$$

where Λ and G are the ionic conductivity and the conductance of the sample, respectively, d represents the distance between two electrodes, and A is the area of the top and bottom electrodes in contact with the sample (i.e., inner diameter of the gasket for solution). The conductivity of the solution did not vary significantly over three days (Supplementary Fig. 10), demonstrating the stability of the solution.

To photoirradiate the materials, we used a 365 nm LED (Dymax Redicure® QX4 LED Head 365nm for the BlueWave® QX4® spot-curing system) as the light source for 2-(4-Methoxystyryl)-4,6-bis(trichloromethyl)-1,3,5-triazine and N-Hydroxyphthalimide triflate. We calibrated the power density of the light source to 0.2 W cm^{-2} with a G&R labs Model 222 intensity meter. Since the other PAGs absorb more strongly at lower wavelengths, we used a white light source (high-pressure mercury bulb, Omnicure S2000 UV Curing system) for N-Hydroxy-5-Norbornene-2,3-dicarboximide perfluoro-1-butanesulfonate, and Triphenylsulfonium Triflate, and calibrated the exposure power density with a Silverline UV Radiometer. We adjusted the light dose by controlling the irradiation duration of the solution. For each PIG solution, we irradiated through a capped Azzota optical glass cuvette while inductively spinning a 6 mm magnetic bar inside to make the solution homogeneous. At specific intervals during irradiation, we removed aliquots from the cuvette and pipetted them into our custom dielectric measurement setup (see above). For the light exposure of PIGel, we made a custom measurement cell. The cell consisted of two parallel, indium tin oxide (ITO)-coated glass plates with a moulded silicon O-ring sealing the PIGel in the middle. A silicone ring has an inner diameter of 25 mm and a thickness of 5 mm and was used as a spacer between the ITO plates. UV irradiation comes through the bottom, transparent ITO to the PIGel. The high optical transmission of the ITO electrode (>90% at 365 nm) facilitated efficient and uniform sample irradiation.

UV–vis absorption spectra test of the solution

We measured the absorption spectra generated from the four photoacids above using their 0.0001 M acetonitrile solutions before and after an 800 J light exposure with an Agilent Cary 7000 Spectrophotometer.

Swelling ratio of PIGels

The swelling behavior of the PIGels was measured gravimetrically. We immersed samples (diameter of 19 mm, thickness of 0.5 mm) in 0.1 M PIG3 DMSO solution at room temperature. At discrete time periods, the gels were removed, placed on a Kimwipe™ to remove surface liquid, and immediately massed.

Mechanical properties of PIGels

We conducted tensile tests on the PIGels using an Instron universal testing system (Model 5943). Briefly, 3 mm PIGel films were initially prepared as described above. Then dogbone samples were cut from this film using an ISO 527-2 (2012), Type 1BA die and Instron CEAST Specimen Preparation Punching Machine. Samples were massed and subjected to appropriate soak in 0.1 M PIG3 DMSO solution (see above). Working quickly to minimize solvent loss, samples were removed from the solution, weighed, and new dimensions (gage thickness and width) measured via calipers. Samples were then marked with two tracking dots, loaded into the pneumatic grips (dP = 4 PSI) and pulled to failure under tensile strain. Strain rates were held constant at 75 mm min^{-1} and strains were measured optically by a video extensiometer (Instron AVE2). We calculate Young's Modulus as the slope in the stress-strain plot over the 5-10% strain regime.

Resolution of photo-patterned ionic conductivity over time

We cut a piece of Clear Flex 50 gel into 3 cm × 4 cm after soaking it in the 0.1 M PIG3 DMSO solution for 90 min. We then illuminate (H_e = 200 J cm^{-2}, λ = 365 nm) a single line (l > 3 mm, w = 5 mm) in the PIGel through a 3D printed photo-mask. Utilizing a custom 3D printed holder for precise alignment, we insert six pins into the gel. In this fixture, three pins are located on top of the irradiated line at a spacing of 1 cm. From the midpoint of the photo-pattern, three other pins are aligned orthogonally at a 1, 2, and 3 cm distance, as shown in Fig. 3a. At each time interval, we connect each pair of pins pairwise to a Keysight E4980AL LCR Meter to measure the local resistance.

PIGels as strain sensors

PUR disks were molded into disks (d = 5 mm, h = 3 mm) similar to the protocols above. After curing, samples were then submersed into a 0.1 M PIG3 DMSO solution for 90 minutes, resulting in a swollen diameter of ~8.32 mm as measured via calipers. The samples were then irradiated (H_e = 140 J cm^{-2}, λ = 365 nm) and loaded onto the Discovery HR-2 hybrid rheometer. We measured the swollen height by reducing the gap between electrodes until an axial force of approximately 0.1 N was observed. Conductance values were measured similar to those above. We then iteratively reduced the gap by 300 microns and measured the corresponding axial force and conductance (see Supplementary Fig. 12 for full data).

Data Availability

The data that support the plots within this paper and other findings of this study are available from the corresponding author upon request.

References

1 Wan, C., Xiao, K., Angelin, A., Antonietti, M. & Chen, X. The Rise of Bioinspired Ionotronics. *Advanced Intelligent Systems* **1**, 1900073 (2019). https://doi.org/10.1002/aisy.201900073

2 Yang, C. *et al.* Ionotronic Luminescent Fibers, Fabrics, and Other Configurations. *Advanced Materials* **32**, 2005545 (2020). https://doi.org/10.1002/adma.202005545

3 Li, C. *et al.* Polyelectrolyte elastomer-based ionotronic sensors with multi-mode sensing capabilities via multi-material 3D printing. *Nat Commun* **14**, 4853 (2023). https://doi.org/10.1038/s41467-023-40583-5

4 Zhu, W., Wu, B., Lei, Z. & Wu, P. Piezoionic Elastomers by Phase and Interface Engineering for High-Performance Energy-Harvesting Ionotronics. *Advanced Materials* (2024). https://doi.org/10.1002/adma.202313127

5 Xu, L. *et al.* A Transparent, Highly Stretchable, Solvent-Resistant, Recyclable Multifunctional Ionogel with Underwater Self-Healing and Adhesion for Reliable Strain Sensors. *Advanced Materials* **33**, 2105306 (2021). https://doi.org/10.1002/adma.202105306

6 Chang, Y. *et al.* First Decade of Interfacial Iontronic Sensing: From Droplet Sensors to Artificial Skins. *Advanced Materials* **33**, 2003464 (2021). https://doi.org/10.1002/adma.202003464

7 Yan, Y. *et al.* Electroactive Ionic Soft Actuators with Monolithically Integrated Gold Nanocomposite Electrodes. *Advanced Materials* **29**, 1606109 (2017). https://doi.org/10.1002/adma.201606109

8 Kotal, M., Kim, J., Kim, K. J. & Oh, I. K. Sulfur and Nitrogen Co-Doped Graphene Electrodes for High-Performance Ionic Artificial Muscles. *Adv Mater* **28**, 1610-1615 (2016). https://doi.org/10.1002/adma.201505243

9 Sun, J. Y., Keplinger, C., Whitesides, G. M. & Suo, Z. Ionic skin. *Adv Mater* **26**, 7608-7614 (2014). https://doi.org/10.1002/adma.201403441

10 Lei, Z., Wang, Q., Sun, S., Zhu, W. & Wu, P. A Bioinspired Mineral Hydrogel as a Self-Healable, Mechanically Adaptable Ionic Skin for Highly Sensitive Pressure Sensing. *Advanced Materials* **29**, 1700321 (2017). https://doi.org/10.1002/adma.201700321

11 Yang, C. H., Chen, B., Zhou, J., Chen, Y. M. & Suo, Z. Electroluminescence of Giant Stretchability. *Advanced Materials* **28**, 4480-4484 (2016). https://doi.org/10.1002/adma.201504031

12 Yang, C. H., Zhou, S., Shian, S., Clarke, D. R. & Suo, Z. Organic liquid-crystal devices based on ionic conductors. *Materials Horizons* **4**, 1102-1109 (2017). https://doi.org/10.1039/c7mh00345e

13 Pawlaczyk, M., Lelonkiewicz, M. & Wieczorowski, M. Age-dependent biomechanical properties of the skin. *Advances in Dermatology and Allergology* **5**, 302-306 (2013). https://doi.org/10.5114/pdia.2013.38359

14 Ogneva, I. V., Lebedev, D. V. & Shenkman, B. S. Transversal Stiffness and Young's Modulus of Single Fibers from Rat Soleus Muscle Probed by Atomic Force Microscopy. *Biophysical Journal* **98**, 418-424 (2010). https://doi.org/10.1016/j.bpj.2009.10.028

15 Niu, C. J. *et al.* Polyacrylamide gel substrates that simulate the mechanical stiffness of normal and malignant neuronal tissues increase protoporphyin IX synthesis in glioma cells. *J Biomed Opt* **20**, 098002 (2015). https://doi.org/10.1117/1.JBO.20.9.098002

16 Keplinger, C. *et al.* Stretchable, Transparent, Ionic Conductors. *Science* **341**, 984-987 (2013). https://doi.org/10.1126/science.1240228
17 Wang, H. *et al.* Ionic Gels and Their Applications in Stretchable Electronics. *Macromolecular Rapid Communications* **39**, 1800246 (2018). https://doi.org/10.1002/marc.201800246
18 Yang, C. & Suo, Z. Hydrogel ionotronics. *Nature Reviews Materials* **3**, 125-142 (2018). https://doi.org/10.1038/s41578-018-0018-7
19 Yiming, B. *et al.* A Mechanically Robust and Versatile Liquid-Free Ionic Conductive Elastomer. *Advanced Materials* **33**, 2006111 (2021). https://doi.org/10.1002/adma.202006111
20 Pu, X. *et al.* Ultrastretchable, transparent triboelectric nanogenerator as electronic skin for biomechanical energy harvesting and tactile sensing. *Science Advances* **3** (2017). https://doi.org/10.1126/sciadv.1700015
21 Wang, J. *et al.* Extremely Stretchable Electroluminescent Devices with Ionic Conductors. *Adv Mater* **28**, 4490-4496 (2016). https://doi.org/10.1002/adma.201504187
22 Wang, S. H., Hou, S. S., Kuo, P. L. & Teng, H. Poly(ethylene oxide)-co-poly(propylene oxide)-based gel electrolyte with high ionic conductivity and mechanical integrity for lithium-ion batteries. *ACS Appl Mater Interfaces* **5**, 8477-8485 (2013). https://doi.org/10.1021/am4019115
23 Bao, G. *et al.* Ionotronic Tough Adhesives with Intrinsic Multifunctionality. *ACS Appl Mater Interfaces* **13**, 37849-37861 (2021). https://doi.org/10.1021/acsami.1c09231
24 Shirai, M. & Tsunooka, M. Photoacid and photobase generators: Chemistry and applications to polymeric materials. *Progress in Polymer Science* **21**, 1-45 (1996). https://doi.org/10.1016/0079-6700(95)00014-3
25 Sun, T., Kang, L., Zhao, H., Zhao, Y. & Gu, Y. Photoacid Generators for Biomedical Applications. *Adv Sci (Weinh)* **11**, e2302875 (2024). https://doi.org/10.1002/advs.202302875
26 Deng, J., Bailey, S., Jiang, S. & Ober, C. K. Modular Synthesis of Phthalaldehyde Derivatives Enabling Access to Photoacid Generator-Bound Self-Immolative Polymer Resists with Next-Generation Photolithographic Properties. *J Am Chem Soc* **144**, 19508-19520 (2022). https://doi.org/10.1021/jacs.2c08202
27 Zhou, W. *et al.* An efficient two-photon-generated photoacid applied to positive-tone 3D microfabrication. *Science* **296**, 1106-1109 (2002). https://doi.org/10.1126/science.296.5570.1106
28 Halbardier, L., Croutxé-Barghorn, C., Goldbach, E., Schuller, A.-S. & Allonas, X. 3D printed objects obtained by combination of radical photopolymerization and photo sol–gel reaction: towards reinforced thermomechanical properties. *Polymer Chemistry* **14**, 4048-4056 (2023). https://doi.org/10.1039/d3py00650f
29 Tsuchimura, T. Recent Progress in Photo-Acid Generators for Advanced Photopolymer Materials. *Journal of Photopolymer Science and Technology* **33**, 15-26 (2020). https://doi.org/10.2494/photopolymer.33.15
30 Zhang, J. *et al.* A known photoinitiator for a novel technology: 2-(4-methoxystyryl)-4,6-bis(trichloromethyl)-1,3,5-triazine for near UV or visible LED. *Polym. Chem.* **5**, 6019-6026 (2014). https://doi.org/10.1039/c4py00770k
31 Anger, C. A. *et al.* Oxasilacycles Leading to UV-Curable Polymers: Synthesis and Application. *Macromolecules* **47**, 8497-8505 (2014). https://doi.org/10.1021/ma501857a

32 Shirai, M. & Okamura, H. i-Line sensitive photoacid generators for UV curing. *Progress in Organic Coatings* **64**, 175-181 (2009). https://doi.org/10.1016/j.porgcoat.2008.08.026
33 Georgiadou, D. G. *et al.* Effect of triphenylsulfonium triflate addition in wide band-gap polymer light-emitting diodes: improved charge injection, transport and electroplex-induced emission tuning. *RSC Advances* **2**, 11786 (2012). https://doi.org/10.1039/c2ra21709k
34 Wright, M. R. *An introduction to aqueous electrolyte solutions*. John Wiley & Sons, (2007).
35 Wang, S.-C. & Tsao, H.-K. Ion Migration through a Polymer Solution: Microviscosity. *Macromolecules* **36**, 9128-9134 (2003). https://doi.org/10.1021/ma034769i
36 A, K. & A, L. Mechanical Behaviour of Skin: A Review. *Journal of Material Science & Engineering* **5** (2016). https://doi.org/10.4172/2169-0022.1000254
37 Lake, G. J. & Thomas, A. G. The strength of highly elastic materials. *Proceedings of the Royal Society of London. Series A. Mathematical and Physical Sciences* **300**, 108-119 (1967). https://doi.org/10.1098/rspa.1967.0160
38 Kolodynska, D. Application of a new generation of complexing agents in removal of heavy metal ions from different wastes. *Environ Sci Pollut Res Int* **20**, 5939-5949 (2013). https://doi.org/10.1007/s11356-013-1576-2
39 Almubarak, T., Ng, J. H., Ramanathan, R. & Nasr-El-Din, H. A. From initial treatment design to final disposal of chelating agents: a review of corrosion and degradation mechanisms. *RSC Advances* **12**, 1813-1833 (2022). https://doi.org/10.1039/d1ra07272b
40 Liao, Y. Design and Applications of Metastable-State Photoacids. *Acc Chem Res* **50**, 1956-1964 (2017). https://doi.org/10.1021/acs.accounts.7b00190

Acknowledgments

The authors acknowledge Tianshu Liu and Tsung-Ching Huang for their support in developing the conductivity characterization experiments.

Author Contributions Statement

T.J.W. conceived the idea of the study. X.L. and S.S. designed the mechanical test setups and fixtures. X.L. and T.J.W. carried out experiments, researched, collected and analyzed data, and drafted the initial manuscript. S.M.A. and W.P. provided technical support and conceptual advice. T.J.W supervised the study. All authors discussed the results and commented on the final manuscript.

Competing Interests Statement

The authors declare no competing interests.

Figure Legends

Fig. 1 | Ionic conductivity measurement and photoacid in DMSO

a, Overview photoacid generators (PAG) and non-ionic photoacid generators (photo-ion generators, PIGs) with the schematic for measuring ionic conductivity. **b,** UV-Vis spectra of MBT, HNT, HNDPB, and TPST (0.0001 M in acetonitrile) before and after UV exposure. **c,** Average (n = 9) ionic conductivity change at f = 1 kHz of 0.1 M MBT, HNT (light source = 365 nm LED), HNDPB, and TPST (light source = Hg lamp) DMSO solution as a function of photo-exposure. **d,** Average (n = 9) ionic conductivity change at f = 1 kHz of 0, 0.1 M, 0.01 M, and 0.001 M MBT in DMSO under photo-exposure (light source = 365 LED). **e,** Average (n = 9) molar conductivity of MBT in DMSO at varying photo-dosages and concentrations showing weak electrolyte behavior, and general behavior of a strong electrolyte.

Fig. 2 | Preparation and properties of PIGels based on Clear Flex 50 with MBT

a, Process for fabricating PIGels. **b,** Swelling behavior of Clear Flex 50 disks (d_0 = 19 mm, h_0 = 0.5 mm) with 0.1M MBT in DMSO solution. **c,** Average (n = 9) conductivity change (f = 1 kHz) of these PIGel with 0, 0.66 wt%, 1.53 wt%, 2.62 wt% PIG concentration as a function of photo-exposure (light source = 365 nm LED). **d,** Young's Modulus of MBT based PIGels before and after 140 J cm^{-2} photo-exposure (light source = 365 nm LED). Error bar represents standard deviation, n = 7. **e,** Ultimate Strain change of MBT based PIGel before and after 140 J cm^{-2} photo-exposure (light source = 365 nm LED). Error bar represents standard deviation, n = 7. **f,** Representative image of compliant PIGel under 12% swelling ratio.

Fig. 3 | Conductivity improvement of different MBT polymer systems

a, Swelling behaviour of Clear Flex 30, 50, and 95 disks (d_0 = 19 mm, h_0 = 0.5 mm) with 0.1M MBT in DMSO solution. **b,** Average (n = 9) conductivity change (f = 1 kHz) of these saturated PIGels after 2800 mins swelling as a function of photo-exposure (light source = 365 nm LED). **c** Comparison of dynamic response and the elastic nature of biological tissue, polymer, composite, and inorganic (left dot is VHB-based PIGel, bottom dot is Clear Flex 95-based PIGel, top dot is Clear Flex 50-based PIGel, central dot represents Clear Flex 30-based PIGel.

Fig. 4 | Demonstration of PIGels

a, Experimental setup for measuring conductive resolution of photo-patterned PIGel. **b,** Resistance change (f = 1 kHz) as a function of time post-irradiation of photo-patterned PIGel. **c,** Average (n = 3) conductance change (f = 1 kHz) of PIGel under deformation. **d,** Schematic of dynamic photo-patterning of a soft, stretchable circuit. **e,** Time series of

photo-patterning of conductivity in a PIGel leading to the progressive illumination of LEDs ($V_{applied}$ = ±100 V, f = 1 kHz).

Editorial Summary

Gel ionotronics are typically easy to prepare, but control of local ionic character is unusual. Here, the authors report the combination of elastomers with photo-ion generators for photopatterned control of conductivity in the gel materials.

Peer review information: *Nature Communications* thanks the anonymous reviewers for their contribution to the peer review of this work. A peer review file is available.